

Received May 12, 2021, accepted May 17, 2021, date of publication May 20, 2021, date of current version May 28, 2021.

Digital Object Identifier 10.1109/ACCESS.2021.3082148

# Internal Parameter Estimation of Lithium-Ion Battery Using AC Ripple With DC Offset Wave in Low and High Frequencies

KWANG SEOK SONG<sup>1</sup>, SUNG-JUN PARK<sup>1</sup>, AND FEEL-SOON KANG<sup>1,2</sup>, (Member, IEEE)

<sup>1</sup>Department of Electrical Engineering, Chonnam National University, Gwangju 61186, South Korea

<sup>2</sup>Department of Electronic Engineering, Hanbat National University, Daejeon 34158, South Korea

Corresponding author: Feel-Soon Kang (feelsoon@hanbat.ac.kr)

This work was supported by the BK21 Program funded by the Ministry of Education and National Research Foundation of Korea under Grant I20SS7608037.

**ABSTRACT** xEV batteries are not easy to accurately estimate and measure aging parameters for reuse due to continuous charging and discharging. In addition, existing AC-IR measurement methods require high-performance micro-controller units (MCUs) to handle complex operations for parametric estimation. As a cost-effective way to solve this problem, we propose AC-IR estimation techniques and implementation circuits to estimate internal battery parameters using AC ripple with DC offset wave in low and high frequencies. It estimates electrolyte resistance ( $R_i$ ) by using band-pass filter (BPF) to extract AC components of a particular frequency voltage and current and by entering very high frequencies that have the effect of shorting the equivalent capacitance by the electrical double layer ( $C_d$ ) of the Randles model. The charge transfer resistance ( $R_d$ ) and electrical double layer capacitance ( $C_d$ ) are estimated by Discrete Fourier transform (DFT), detecting effective and reactive current by inserting low frequencies. To realize the proposed approach, we propose analog power measurements and peak detection circuits, and a circuit configuration of converter supplying AC ripple with DC offset wave to estimate internal parameters at the same time to charge battery. To verify the feasibility and high-performance of the proposed AC-IR estimation method, we carry out PSIM simulations and experiments, and compare results with commercial battery parameter measuring instrument. As a result, we found that the error rate of the proposed method is lower than that of the commercial instrument as  $R_i$  is 0.24% and  $R_d$  is 1.18%, respectively.

**INDEX TERMS** Alternating current internal resistance (AC-IR), band-pass filter (BPF), direct current internal resistance (DC-IR), discrete fourier transform (DFT), end of life (EOL), Randles model, state of charge (SOC), state of health (SOH).

## NOMENCLATURE


### A. ABBREVIATIONS

<b>AC-IR</b>	alternating current internal resistance
<b>ADC</b>	analog-to-digital converter
<b>BMS</b>	battery management system
<b>BPF</b>	band-pass filter
<b>CC-CV</b>	constant current and constant voltage
<b>CE</b>	calculation engine
<b>DC-IR</b>	direct current internal resistance
<b>DFT</b>	discrete Fourier transform
<b>EOL</b>	end of life
<b>EV</b>	electric vehicle
<b>LPF</b>	low-pass filter

<b>MCU</b>	micro-controller unit
<b>PGA</b>	programmable gate array
<b>PLL</b>	phase-locked loop
<b>PWM</b>	pulse width modulation
<b>SOC</b>	state of charge
<b>SOH</b>	state of health

### B. SYMBOLS

$A_{pp}$	maximum apparent power
$C_d$	electrical double layer capacitance
$I_1$	battery charging current with Level 1
$I_2$	battery charging current with Level 2
$i_d$	effective current
$i_q$	reactive current
$P$	effective power

The associate editor coordinating the review of this manuscript and approving it for publication was Sze Sing Lee .

$Q$	reactive power
$P_{max}$	maximum power
$P_{min}$	minimum power
$R_d$	charge transfer resistance
$R_i$	electrolyte resistance
$R_{dc}$	internal resistance of battery
$ S $	apparent power
$\theta$	phase difference
$V_{base}$	base DC input voltage of the converter
$V_{ocv}$	internal open-circuit voltage of battery
$V_{out}$	output voltage of the converter
$V_{PWM}$	high frequency AC ripple with DC offset wave
$Z_b$	impedance line of battery

## I. INTRODUCTION

Waste Lithium-ion batteries are expected to surge as xEVs are rapidly increasing worldwide, but recycling systems for second-use are very insufficient. In the industry, state of health (SOH) estimation technique generally uses battery discharge capacity; to make such estimate, definition of end of life (EOL) of battery is needed. Usually, discharge capacity rate of battery EOL is defined at 80%, a capacity not resulting in dangers during vehicle operation. For accurate calculation of SOC (state of charge), an important parameter for controlling charging and discharging in BMS (Battery Management System), compensations using discharge capacity - the information on SOH, or the aging, of battery - are required. Battery modeling and measurements and diagnosis of various parameters are important to estimate SOC and SOH of the battery [1]–[9]. Since the batteries used in xEVs have complex physical chemical reactions in the battery cells, the conventional deterministic methods Model-based and Data-based SOH estimation methods are very difficult to accurately estimate SOH. Furthermore, it is not possible to capture the stochastic nature of the battery aging process under use [10]. The SOH of discarded batteries is highly nonlinear, and traditional decomposition trend data is limited. Therefore, achieving accurate and effective SOH estimation remains a challenging task [11]. To be practical, SOH estimation methods must be practicable at the battery pack or EV level as well as at the individual cell level [12].

To utilize the second-use xEV battery modules, studies including precise internal parameter estimation are being researched [13]–[25]. DC-IR is a widely used method to measure internal resistance against each terminal voltage and current based on Randles model. It estimates charge transfer resistance ( $R_i$ ), which refers to the potential loss that occurs when charge generated by chemical reaction at battery electrode is transferred out of the battery. Diffusion resistance ( $R_d$ ), which is an equivalent of electrochemical reaction on surface of electrode, and capacitance of electric double layer ( $C_d$ ) is used to accurately estimate parameters in xEV re-useable batteries. However, due to continuous charging and discharging, it is not easy to measure electrical parameters of batteries, and as aging of the battery accelerates by cause of high ambient temperature and high charging and

discharging current, there is a limit to estimate the internal resistance [13]–[20]. Another method measures AC voltage by applying AC current on battery cell for 1~5 seconds at a frequency of  $1.0 \pm 0.1$  kHz. All voltage measurements must be performed on a cell terminal independent from current flow. In estimating charge transfer resistance ( $R_i$ ), which refers to charge loss close to measurement of impedance at a designated frequency that is identical with approximate resistance, AC current should be applied so that peak voltage is maintained at 20mV or lower. Square roots, squares, divisions, and cosine functions are performed on MCU to calculate the effective, reactive components and power factor. This is made under the assumption that the ratio of sampling frequency against power measurement frequency is extremely large when measuring power from integration of values quantified through an ADC (analog-to-digital converter). If power measurement frequency is so fast that there are a smaller number of sampling in a period, measurement resolution becomes lower, hence a high-speed microprocessor is required in proportion to measurement frequency [21]–[25].

Power measurement method based on effective value is suitable when measurement frequency is lower than sampling frequency, but the higher the frequency of measurement, the lower the utility of the method. In particular, when measurement frequency is higher than sampling frequency, it becomes impossible to measure power. As a cost-effective way to solve this problem, we propose AC-IR estimation techniques and implementation circuits to estimate internal battery parameters using AC ripple with DC offset wave in low and high frequencies. It estimates electrolyte resistance ( $R_i$ ) by using band-pass filter (BPF) to extract AC components of a particular frequency voltage and current and by entering very high frequencies that have the effect of shorting the equivalent capacitance by the electrical double layer ( $C_d$ ) of the Randles model. The charge transfer resistance ( $R_d$ ) and electrical double layer capacitance ( $C_d$ ) are estimated by Discrete Fourier transform (DFT), detecting effective and reactive current by inserting low frequencies. To realize the proposed approach, we propose analog power measurements and peak detection circuits, and a circuit configuration of converter supplying AC ripple with DC offset wave to estimate internal parameters at the same time to charge battery. To verify the feasibility and high-performance of the proposed AC-IR estimation method, we carry out PSIM simulations and experiments, and compare results with commercial battery parameter measuring instrument.

## II. BATTERY PARAMETER ESTIMATION TECHNIQUES

### A. DC-IR MEASUREMENT

Fig. 1(a) shows the Randles model, i.e., the most common method to measure DC-IR. Here,  $R_i$  is electrolyte resistance,  $R_d$  is charge transfer resistance, and  $C_d$  is an equivalent capacitance by electric double layer. As battery's internal resistance and serial impedance components include temperature characteristics, they cannot be set to a certain value

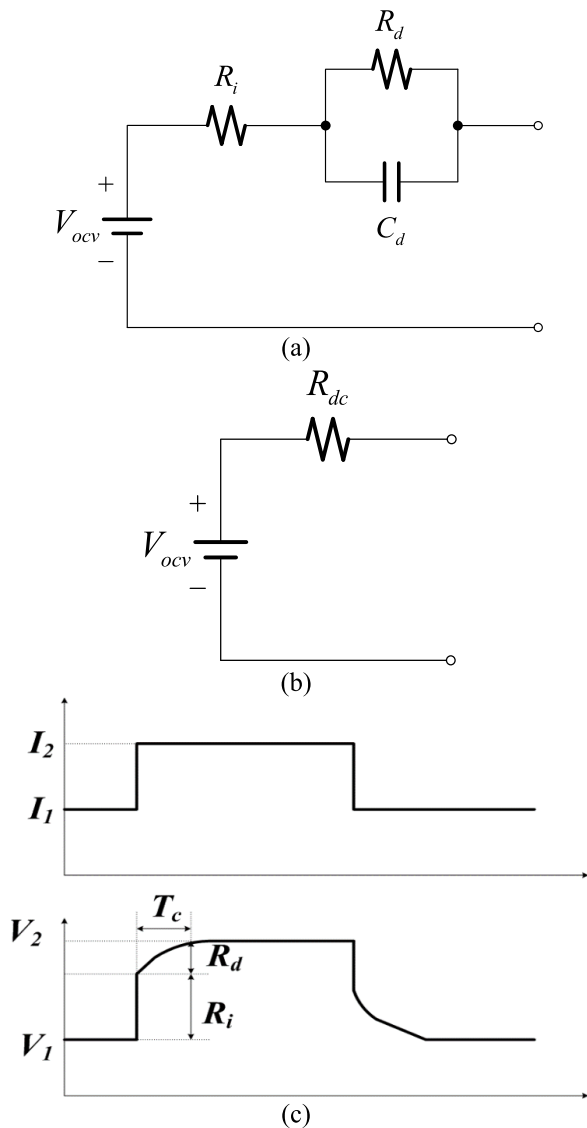


**FIGURE 1.** Randles model and DC-IR measurement, (a) Randles model, (b) simplified Randles model, (c) Estimation of internal resistance ( $R_{dc}$ ) of battery by pulsed DC consisting of two-level constant current in battery charging mode.

during battery charging. In Fig. 1(a), when discharging, capacitance is shorted by capacitance  $C_d$  and the circuit operates with resistance  $R_i$  only; in normal constant current charging mode, capacitance is deemed to be open, the circuit operates with the sum of resistances  $R_i$  and  $R_d$ . And  $C_d$  can be calculated from time constant. Therefore, information necessary for battery modeling during constant current charging can be obtained with just the internal resistance and the sum of resistances  $R_i$  and  $R_d$ .

Battery’s internal voltage ( $V_{ocv}$ ) and SOC share linear relationship and a simplified equivalent circuit model in Fig. 1(b) can be used to estimate internal voltage during constant current charging. In a pulsed DC technique consisting of two-level constant charging current, Level 1 ( $I_1$ ) is identical with the prior constant current for battery charging, whereas

Level 2 ( $I_2$ ) is added to track battery parameters in real time as shown in Fig. 1(c). Battery’s internal voltage is defined as:

$$V_{ocv} = V_1 - R_{dc}I_1 = V_2 - R_{dc}I_2 \quad (1)$$

In battery charging mode with two-level constant current,  $R_{dc}$  can be estimated and calculated as:

$$R_{dc} = R_i + R_d = \frac{V_1 - V_2}{I_1 - I_2} \quad (2)$$

In two-level constant current charging, the period of each current level must be longer than time constant. The larger the difference in currents of the levels, the more precise the measurement is possible. However, internal resistance changes according to level of charging current and DC-IR uses only the information on the sum of two resistances in Randles model equivalent circuits, making it difficult to guarantee the precision of battery characteristics.

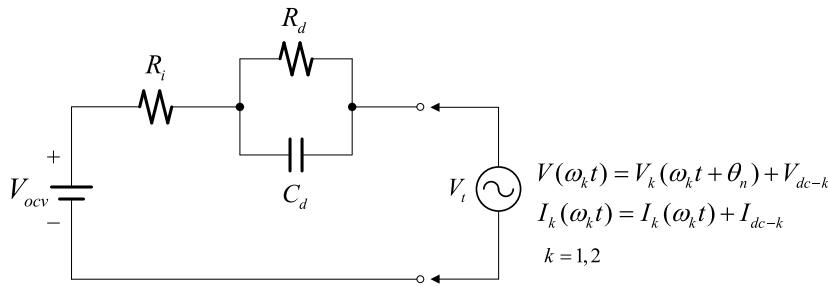
**B. AC-IR MEASUREMENT**

In general, AC-IR Measurement uses two frequencies between 10mHz and 1kHz to measure impedance, and the injected frequencies are no larger than 5% of charging charge capacity to guarantee its linearity. At this time, response voltage is within 20~0mV and internal resistance is estimated by leaving the battery to rest for 2 hours after each charging stage.

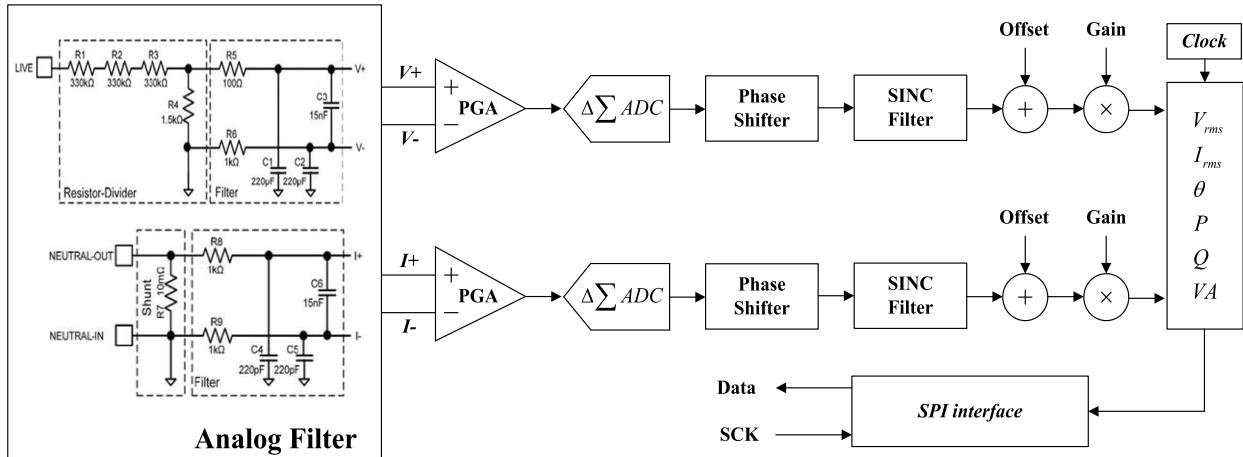
Fig. 2 shows an equivalent circuit for Randles model and a block diagram of power measurement for traditional AC-IR estimation. Sensors can be configured differently according to power measurement situations, but normally they consist of analog filters that include voltage dividing resistors and current sensing resistors, and it is desirable to set cut-off frequency at least 10 times higher than AD sampling frequency. In these type of digital power measurements, when frequency of measurement object is similar with sampling frequency, power measurement is practically unachievable. In the end, MCU (micro-controller unit) needs to calculate square roots, squares, divisions, and cosine functions and this enables power measurements using quantized values using an AD converter. In addition, when there are few samplings in a measurement cycle due to high power measurement frequencies, the resolution becomes low, hence a high speed MCU is required in proportion to power measurement frequencies. Theoretically Nyquist frequency requires sampling frequency to be at least twice of measurement frequency; however, in practice, sampling frequency needs to be at least a hundred times higher than measured frequency and when measured frequency is high, then the MCU needs to be able to sample at very high speeds.

**III. PROPOSED AC-IR ESTIMATION TECHNIQUES**

A circuit with structure to detect certain high frequency by applying AC ripple with DC offset wave at terminal can be changed to an AC component equivalent circuit as shown in Fig. 3. DC offset wave having AC ripple contains various high frequencies and can detect a specific frequency through



(a)



(b)

FIGURE 2. Conventional AC-IR measurement, (a) Randles model with two frequencies, (b) Block diagram for power measurement.

BPF (band-pass filter). Filter design and gain value adjustment enables detection of a certain frequency.

In Fig. 3(a), normal output voltage and current of PWM converter for charging batteries are expressed by DC component and high frequency term which is a multiple of switching frequency.

$$v_{in} = v_{dc} + V_1 \sin(\omega_1 t) + V_3 \sin(3\omega_1 t) + \dots \quad (3)$$

$$i_{in} = i_{dc} + I_1 \sin(\omega_1 t + \theta_1) + I_3 \sin(3\omega_1 t + \theta_2) + \dots \quad (4)$$

After applying BPF, it can detect only the fundamental frequency component from voltage and current:

$$v_1 = V_1 \sin(\omega_1 t + \phi_1) \quad (5)$$

$$i_1 = I_1 \sin(\omega_1 t + \theta_1 + \phi_1) \quad (6)$$

In the equivalent circuit given in Fig. 3(b), impedance line ( $Z_b$ ) is expressed as follows:

$$Z_b = R_i + R_d \parallel \frac{1}{j\omega C_d} \quad (7)$$

A practically infinite frequency for high frequency AC-IR estimation is impossible and  $R_i$  is estimated by applying a high frequency component where capacity reactance practically becomes zero. For low frequency AC-IR estimation,

$R_d$  and  $C_d$  values are estimated by applying low frequency components and separating them into effective and reactive components.

A power measurement method which can measure power due to detection of maximum and minimum instantaneous power is proposed, which measure power accurately regardless of measuring frequency. Normal output voltage and current of power converter for charging batteries are consisted of DC component and high frequency term. Here, DC component plays a role to charge battery and high frequency component is for AC-IR estimation and has no relations with charging amount. It is difficult to measure power when measurement frequency is higher than sampling frequency. To overcome this problem, we propose a new power measurement method based on peak value for selection of high frequency.

Fig. 5 shows the block diagram for power measurement by detection of maximum and minimum instantaneous power proposed in this paper. Low-pass filter is used to remove high frequency components in voltage and current, cut-off frequency of all filters is set at measurement frequency to solve compensation for phase delay and attenuation of measurement signal is compensated. Voltage and current signal which passes the filter will produce instantaneous power

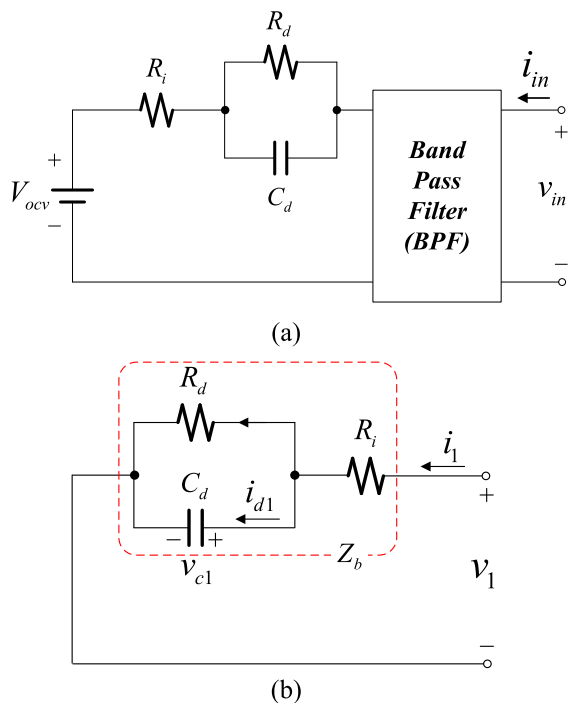


**FIGURE 3.** Modification of Randles model for the proposed AC-IR estimation, (a) Randles model with BPF, (b) Equivalent circuit after applying BPF.

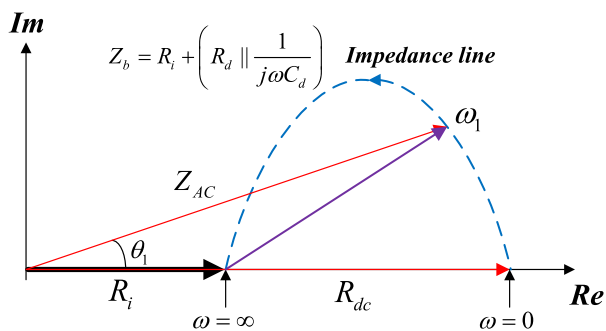


**FIGURE 4.** Impedance trajectory for the proposed AC-IR estimation.

using analog multiplier, analog instantaneous power signal will detect maximum value using maximum value detection circuit and minimum value detection circuit will detect minimum value. Detected maximum and minimum analog values are quantized by ADC and will pass digital filter, after which a frequency information with practically zero reactance power will be obtained at CE (calculation engine). Assuming that voltage and current are sine curves with phase difference of  $\theta$ , then the current will be separated into sine and cosine terms as:

$$v(t) = \sqrt{2}V \sin(\omega t) \tag{8}$$

$$i(t) = \sqrt{2}I \sin(\omega t - \theta) = \sqrt{2}I [\cos \theta \sin \omega t - \sin \theta \cos \omega t] \tag{9}$$

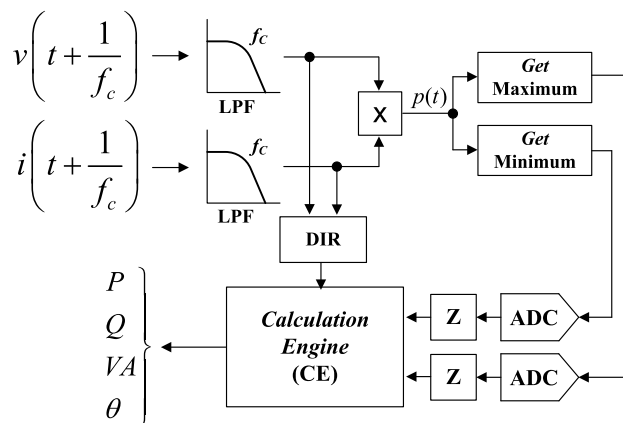


**FIGURE 5.** Block diagram on peak power detection for selection of high frequency ( $Q \approx 0$ ).

In (9), the current component which is in phase with the voltage is separated to effective current component, and the current component with  $90^\circ$  phase difference with the voltage is separated to reactive current component as:

$$i_d(t) = \sqrt{2}I \cos \theta \sin \omega t \tag{10}$$

$$i_q(t) = \sqrt{2}I \sin \theta \cos \omega t \tag{11}$$

Due to current which is separated into effective and reactive components, power is expressed in instantaneous effective and reactive power as:

$$P = VI \cos \theta \tag{12}$$

$$Q = -VI \sin \theta \tag{13}$$

To find effective and reactive power, information on effective values and phase difference of voltage and current are necessary.

$$p(t) = \frac{A_{pp}}{2} \cos \theta + \frac{A_{pp}}{2} \cos(2\omega t + \theta) \tag{14}$$

(14) was expressed to measure power with peak values: Here,  $A_{pp}$  ( $= V_p I_p$ ) is the apparent power, and the lower subscript ( $p$ ) means the peak value.

From Fig. 6, the relationship between effective power and maximum and minimum instantaneous power are as:

$$P = \frac{A_{pp}}{2} \cos \theta = \frac{p(t)_{\max} + p(t)_{\min}}{2} \tag{15}$$

In addition, the relationship between apparent power and maximum and minimum instantaneous power are as:

$$|S| = \frac{p(t)_{\max} - p(t)_{\min}}{2} \tag{16}$$

From (15) and (16), reactive power is obtained as:

$$Q = \sqrt{|S|^2 - P^2} \tag{17}$$

The phase difference between voltage and current is given as:

$$\theta = \cos^{-1} \left( \frac{P}{|S|} \right) \tag{18}$$

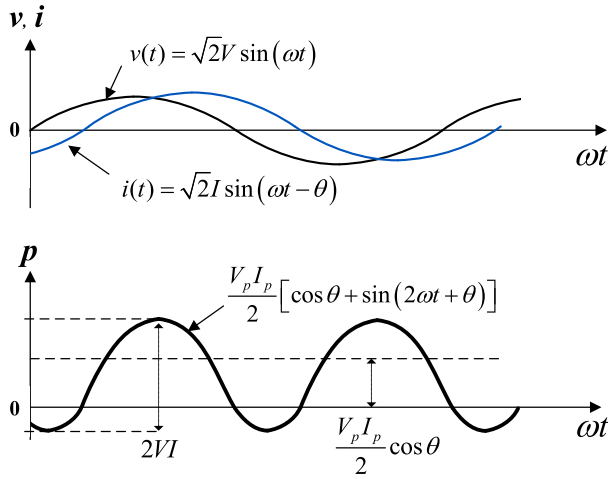


FIGURE 6. Principle of power measurement by using peak values.

Therefore, if the information on maximum and minimum instantaneous power can be obtained, then phase information can be calculated using (18). For the purpose of selecting a plausible power source with a phase  $\theta$  close to zero, the power condition under which voltage and current needs to be in phase is as follows:

$$\begin{aligned} |S|_1 &\approx P_1 \approx V_1 I_1 \\ Q_1 &\approx 0 \\ P_1 &\geq 0.95 V_1 I_1 \end{aligned} \quad (19)$$

Fig. 7 shows a circuit to detect the maximum power ( $P_{max}$ ). It is operated to detect peak power through comparison of input power, detect positive polarity by diode, maintain charging capacity of  $C_t$  by producing output when its capacity is exceeded and resetting before the next high frequency signal input.

Fig. 8 shows a circuit to detect minimum power ( $P_{min}$ ). It is operated to detect peak power through comparison of input power, detect negative polarity by diode, maintain charging capacity of  $C_t$  by producing output when its capacity is exceeded and resetting before the next high frequency signal input.

Fig. 9 shows the block diagram for the proposed parameter extraction using high frequency. Charge transfer resistance ( $R_d$ ) is extracted using peak value detection circuit through selected high frequency measurement input. A high frequency from peak value detection circuit with  $Q$  close to zero is injected, and high frequency is extracted to calculate electrolyte resistance ( $R_i$ ) through peak value calculations. AC ripple with DC offset wave is injected through PWM converters and the source which is in phase with AC voltage and AC current passes through BPF filter to detect high frequency. The AC ripple with DC offset wave is shown in Fig. 9(a) and expressed as:

$$v_{in}(t) = v_{ac}v(t + f_n) + V_{dc} \quad (20)$$

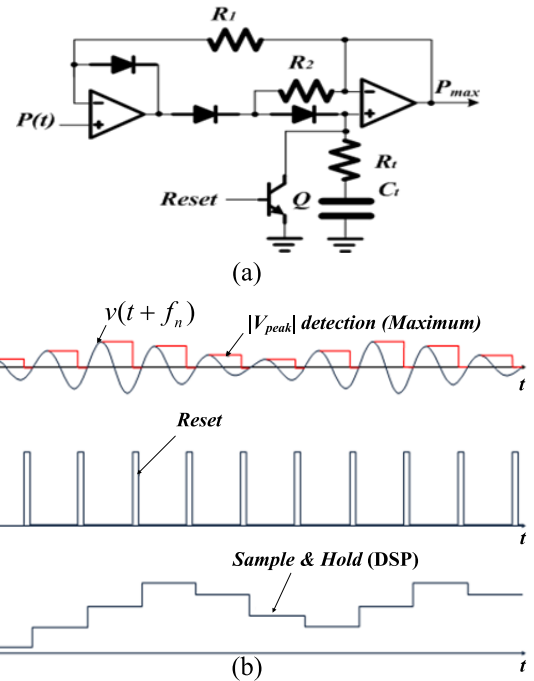


FIGURE 7. Maximum power  $P_{max}$  detection, (a) Circuit configuration, (b) Key waveforms.

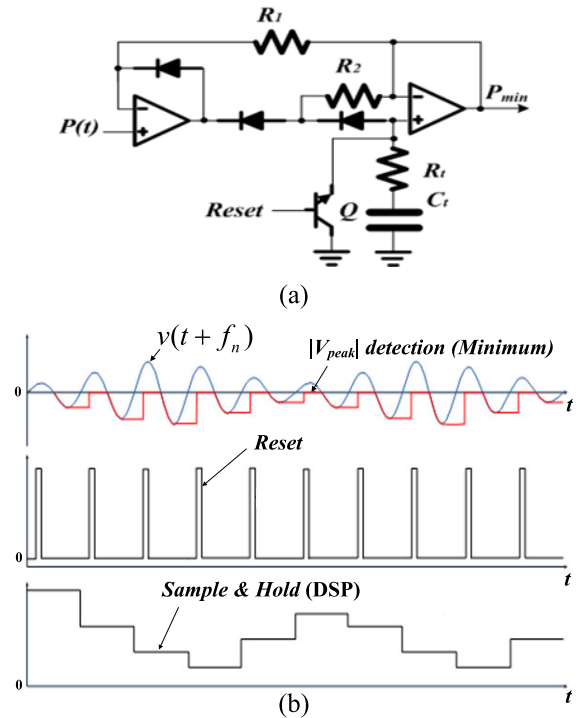
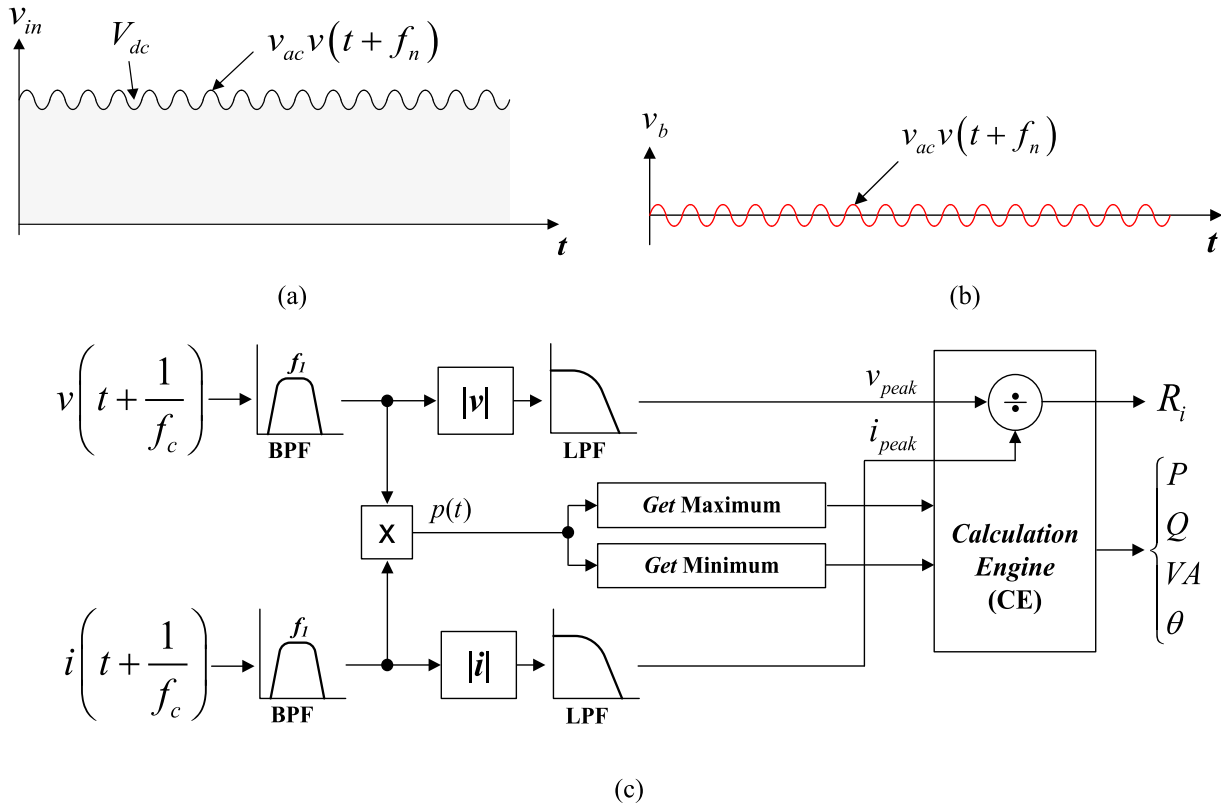


FIGURE 8. Minimum power  $P_{min}$  detection, (a) Circuit configuration, (b) Key waveforms.

In Fig. 9(b), the voltage and current are extracted from the AC ripple with DC offset wave as:

$$v_b(t) = v_{ac}v(t + f_n) \quad (21)$$



**FIGURE 9.** High frequency component extraction and control block diagram, (a) AC ripple with DC offset wave by PWM converter, (b) BPF filtering to detect high frequency, (c) Control block diagram for estimation of electrolyte resistance ( $R_i$ ).

$$i_b(t) = i_{ac}i(t + f_n) \tag{22}$$

After extracting analog peak from voltage and current, electrolyte resistance ( $R_i$ ) is obtained by:

$$R_i = \frac{v_{peak}}{i_{peak}} = \frac{v_{ac}}{i_{ac}} \tag{23}$$

Fig. 10(a) is the result of performing discrete Fourier transform (DFT) on current based on the voltage phase. It shows the phase difference between voltage and current and the process of separating current into effective ( $i_d$ ) and reactive ( $i_q$ ) currents.  $v_c(t)$  value is calculated to detect voltage phase angle as given in Fig. 10(b).

In Fig. 10(b), after  $R_i$  is measured using high frequency, voltage across the parallel connected  $R_d$  and  $C_d$  is expressed by (24). Here, the lower subscript ( $p$ ) means the peak value.

$$v_C = v_{1p} - R_i i_1 = V_{cp} \sin(\omega t + \phi_1) \tag{24}$$

At this time, when fundamental component is expressed in Fourier series expansion of battery current based on the phase of capacitor voltage, it can be defined as:

$$i_1(t) = I_{1p} [\cos(\theta) \sin(\omega t + \phi_1) - \sin(\theta) \cos(\omega t + \phi_1)] \tag{25}$$

From (25), effective current term ( $I_d$ ) which is in phase with voltage and reactive current term ( $I_q$ ) has a phase difference of  $90^\circ$  with voltage can be derived as:

$$i_d(t) = I_d \cos(\omega t + \phi_1) \tag{26}$$

$$i_q(t) = I_q \sin(\omega t + \phi_1) \tag{27}$$

In the proposed AC-IR measurement, effective component  $R_d$  which is a charge transfer resistance is estimated as:

$$R_d = \frac{V_{cp}}{I_{qp}} \tag{28}$$

Reactive component  $C_d$  which corresponds to the capacitance of electric double layer can be defined as:

$$C_d = \frac{V_{cp}}{\omega I_{qp}} \tag{29}$$

Fig. 11 shows the block diagram for the proposed AC-IR parameter estimation. Low frequency which corresponds to the voltage and current of control power supply injected into the battery detects signals within 1Hz and performs analog to digital conversion using MCU through adequate gain in filter. Voltage phase is detected through PLL (phase-locked loop) and current is separated into effective and reactive components so as to enable extraction of  $R_d$  (charge transfer resistance) and  $C_d$  (capacitance of electric double layer) parameters. As shown in Fig. 11, PLL is applied to voltage to detect phase angle. By applying DFT algorithm based on the voltage phase, current information is calculated, and  $R_d$  and  $C_d$  are estimated.

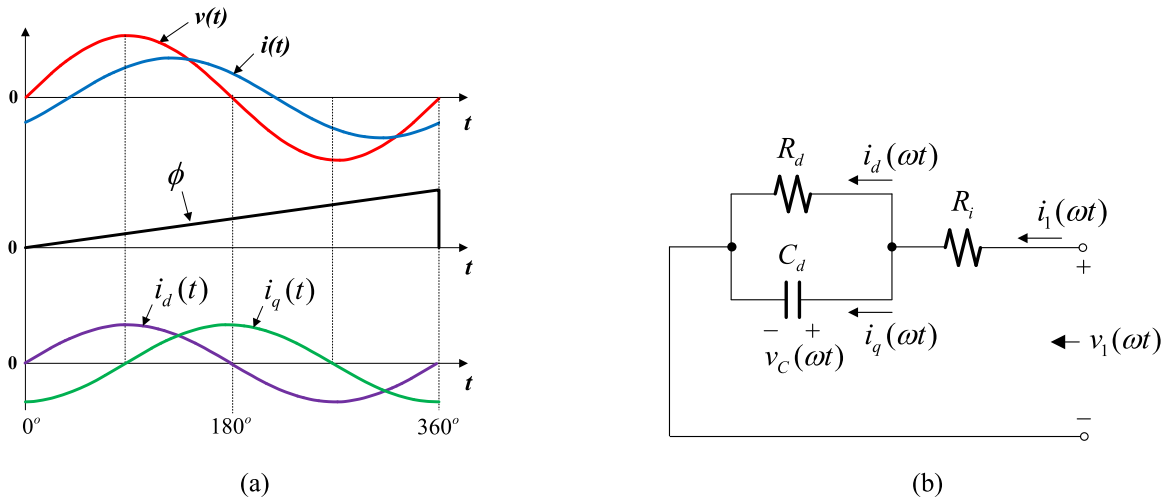


FIGURE 10. Parameter estimation using effective and reactive current separation, (a) Current DFT based on voltage phase angle, (b) AC-IR equivalent circuit according to low frequency input.

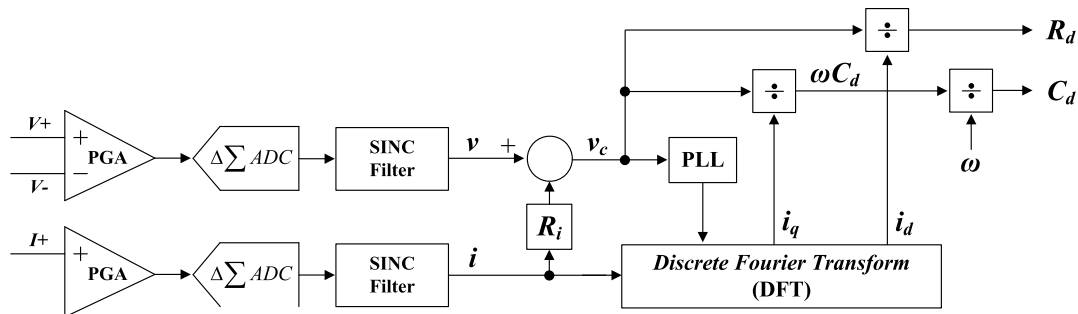


FIGURE 11. Block diagram for estimation of charge transfer resistance ( $R_d$ ) and capacitance of electric double layer ( $C_d$ ).

IV. SIMULATION AND EXPERIMENT RESULTS

Fig. 12 shows the power conversion stage and control flowchart for the proposed AC-IR estimation while charging battery. Upper part configures high frequency source, lower part configures power supply for battery charging. Output current is detected using LC filter and current sensor.  $V_{out}$  integrates high frequency switching power ( $V_{PWM}$ ) for AC ripple with DC offset wave and base DC input ( $V_{base}$ ).

Fig. 13 shows simulation result to estimate an electrolyte resistance ( $R_i$ ). Gain is set to 100 and BPF frequency is configured to 10kHz to match with alternating frequency of high switching frequency. Therefore, high frequency on voltage and current from alternating wave injected by AC ripple with DC offset wave is detected and used as the source for peak value detection. In the peak detection given in Fig. 9, the peak is detected using absolute values and LPF (cut-off 1 kHz) and  $R_i$  is estimated using (23) in a range that is close to  $Q \approx 0$ . In the simulation,  $R_i$  was set to  $0.85\Omega$ . From the result, we can find that the proposed approach is working well for  $R_i$  estimation.

When the vertical fluctuation waveform is input in Fig. 7(a), the circuit detects maximum value continuously due to the reset function as shown in Fig. 14(a). When the

vertical fluctuation waveform is input in Fig. 8(a), the circuit detects minimum value continuously due to the reset function as shown in Fig. 14(b).

Fig. 15 shows simulation result to estimate  $R_d$  and  $C_d$ . It can be confirmed that results agree with  $R_d$  and  $C_d$  setting values through DLL calculations. Ultimately, this has its strength in easy configuration based on cut-off frequency selection of sensor block and internal calculations. In the simulation,  $R_d$  and  $C_d$  of battery were set to  $3.6\Omega$  and  $2000\mu F$ , respectively. From the result, we can notice that the proposed approach is working well for  $R_d$  and  $C_d$  estimation.

A. EXPERIMENTS

Fig. 16 shows an experimental set-up for the proposed AC-IR measurement. It consists of battery charger with BMS, AC-IR estimation board, display part, and Lithium-ion battery. Table 1 shows the specifications of Lithium-ion battery. Table 2 lists up the specifications of charger and AC-IR measurement board. For system operation, DC converter with soft-start function is operated to generate base DC voltage ( $V_{base}$ ), then AC ripple with DC offset voltage is formed by PWM converter switching operation to perform battery charge and AC-IR measurement. Li-ion batteries usually



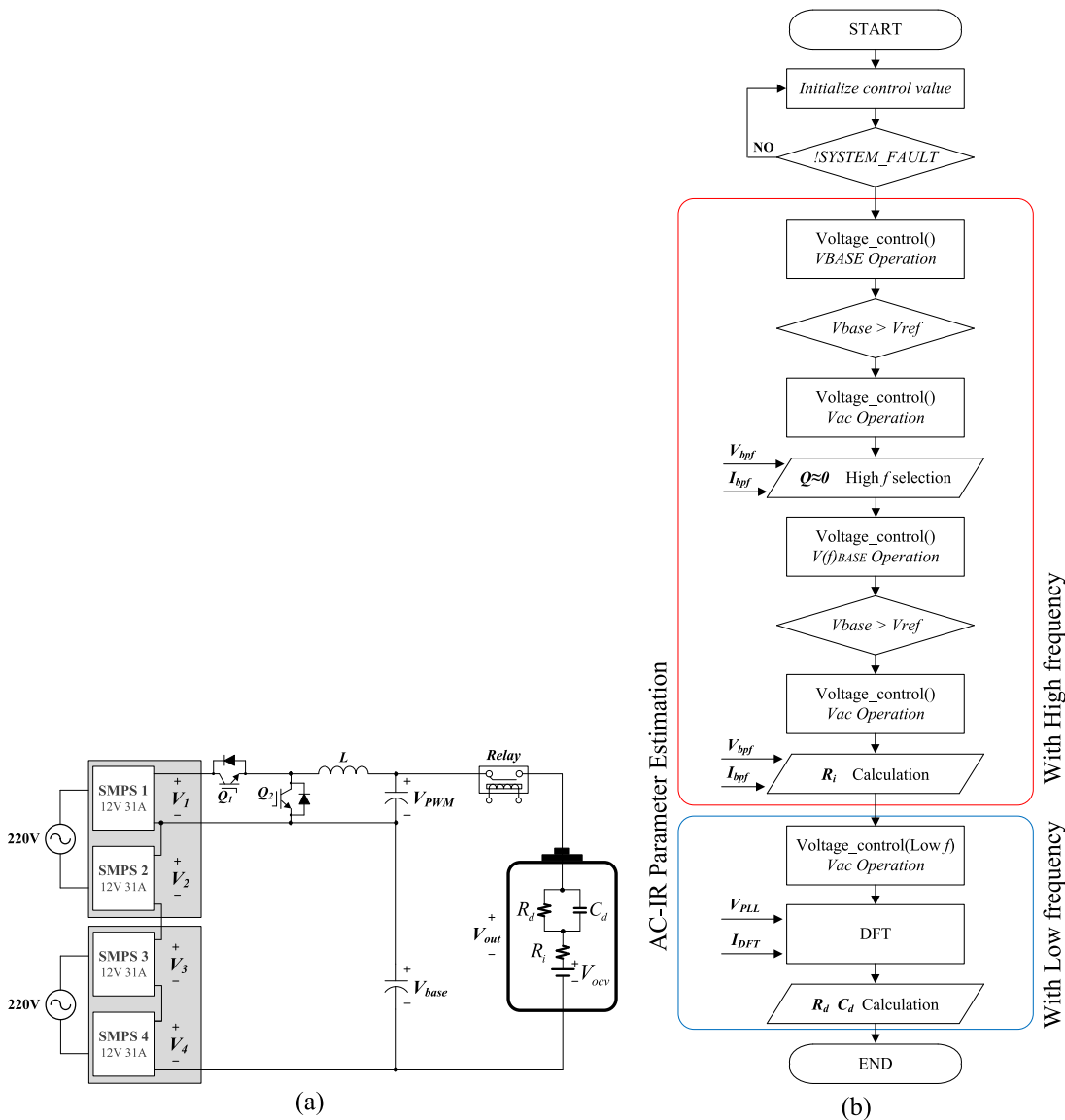


FIGURE 12. Power conversion stage and control flowchart for the proposed AC-IR estimation while charging battery, (a) Power conversion stage, (b) Control flowchart.

allow current ripple of less than 3% because larger charging current ripple reduces the life-cycle of the battery. Thus, the charging current ripple of the converter is also limited to less than 3%. Resistive load is configured for discharging battery and is connected using a terminal block.

Fig. 17(a) shows the experiment waveform to check the standby operation and charging voltage to charge a lithium-ion battery with nominal voltage of 32V at standby with voltage of 30.5V. DC power source of the charger is configured with base voltage ( $V_{base}$ ) and control voltage ( $V_{PWM}$ ) for low and high frequency responses, respectively. Initial standby voltages of converter for base voltage and control voltage are set at 15V and 5V respectively, and as shown in Fig. 17(a), at standby state, converter voltage maintains at set value. At time  $t_1$ , battery is connected. Then controller detects battery voltage, a voltage corresponding to 80% of

TABLE 1. Specifications of Lithium-ion battery.

Item	Specifications
Energy (Normal)	822 Wh
Capacity (Normal)	27.4 Ah
Voltage	30 V (3.75 V per cell)
Battery module configuration	1P8S (1 parallel & 8 series)
Weight	6.5 kg
xEV	LF/JF PHEV

battery voltage becomes the command value for output voltage of base converter ( $V_{base-ref}$ ) and a voltage corresponding to 30% of battery voltage becomes the command value

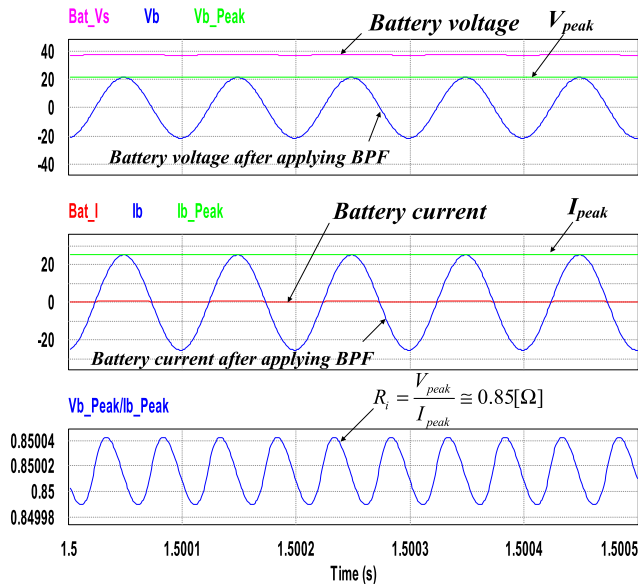


FIGURE 13. Estimation of electrolyte resistance ( $R_j$ ) using peak value.

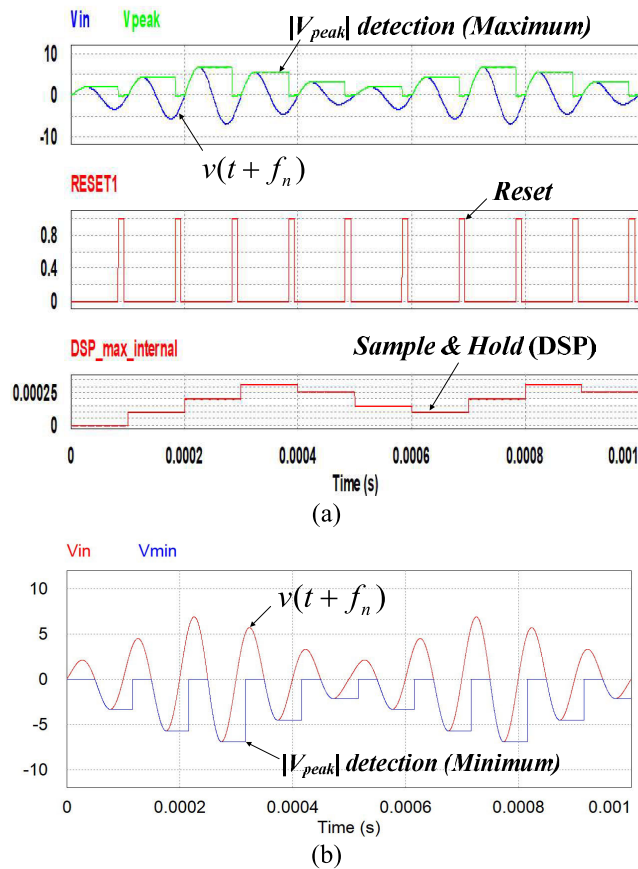


FIGURE 14. Continuous peak detection to obtain maximum and minimum value, (a)  $V_{max}$ , (b)  $V_{min}$ .

for output voltage of control converter ( $V_{PWM-ref}$ ). Output voltages of each converter have time constant of 120ms and 160ms respectively and stably operate at 24.4V and 9.15V

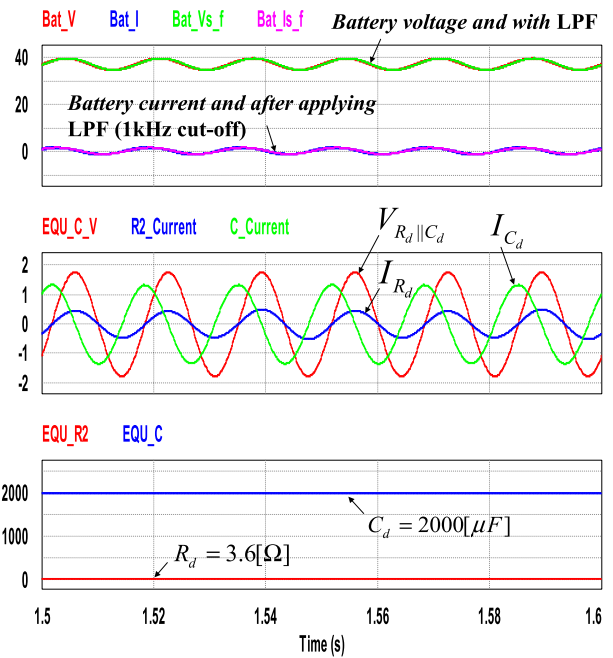


FIGURE 15. Estimation of charge transfer resistance ( $R_d$ ) and electric double layer capacitor ( $C_d$ ).

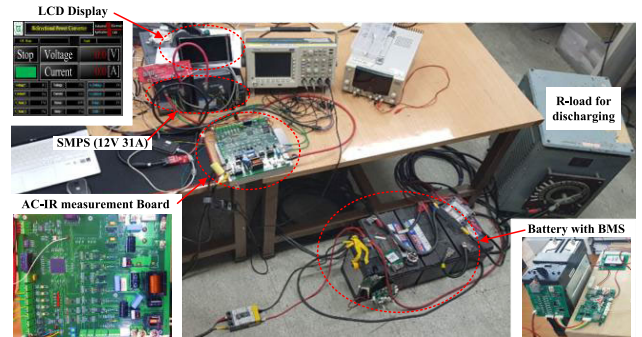
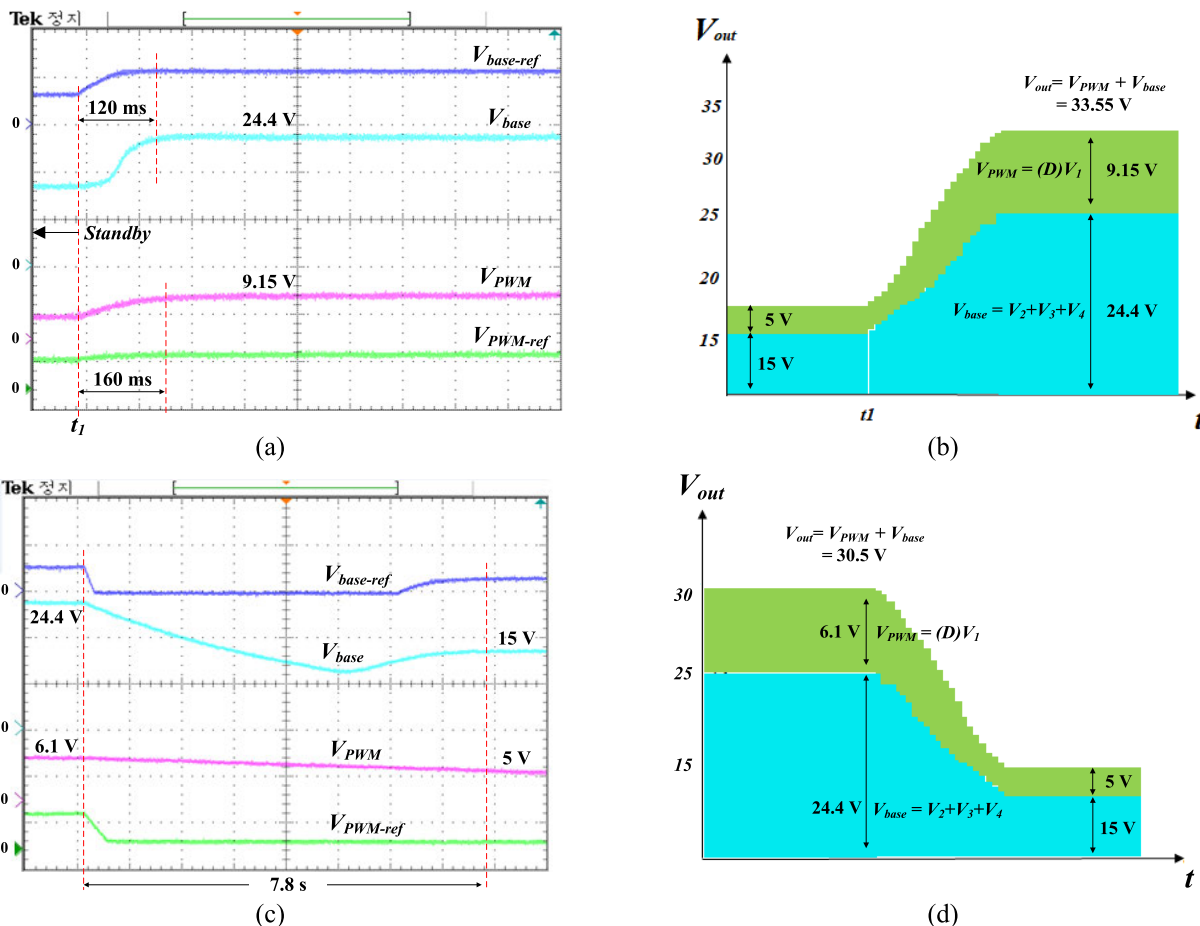


FIGURE 16. Experimental set-up for the proposed AC-IR estimation while charging battery.

respectively as shown in Fig. 17(b). Fig. 17(c) shows the experimental result with changes in base voltage ( $V_{base}$ ) and control voltage ( $V_{PWM}$ ) of the converter when the battery is returned to standby state after charging completely. Output voltages of each converter have time constant of 7.8s and stably operate at 15V and 5V respectively as shown in Fig. 17(d).

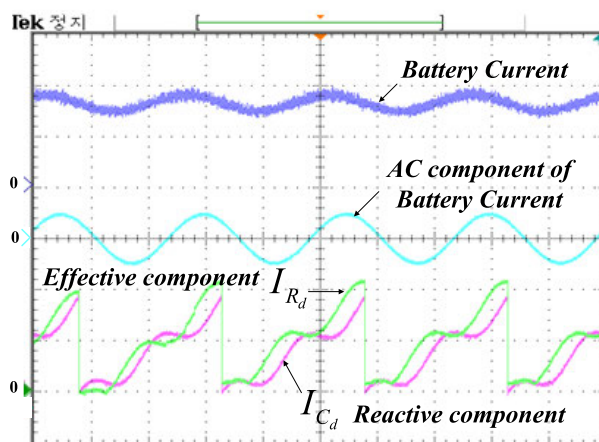
Fig. 18 shows the experimental waveform to check separation of effective and reactive currents to perform DFT on detected low frequency AC current of a battery charger. A control voltage is injected, and AC component of the battery current is extracted. Considering the gain by differential input, the converter receives ADC input, and the current is separated into effective and reactive currents using DFT in MCU. During charging, control voltage is set to 5V and in CC-CV mode the converter operates in preset value. Through digital filtering on AC frequency, the current is separated



**FIGURE 17.** Experimental results for  $V_{base}$  and  $V_{PWM}$  when battery charging mode from standby state and vice-versa, (a) From standby state to charging mode, (b) Variation of output voltage in converter, (c) Returning to standby mode after charging is complete, (d) Variation of output voltage in converter when returning to standby state.

**TABLE 2.** Specifications for charger and AC-IR measurement board.

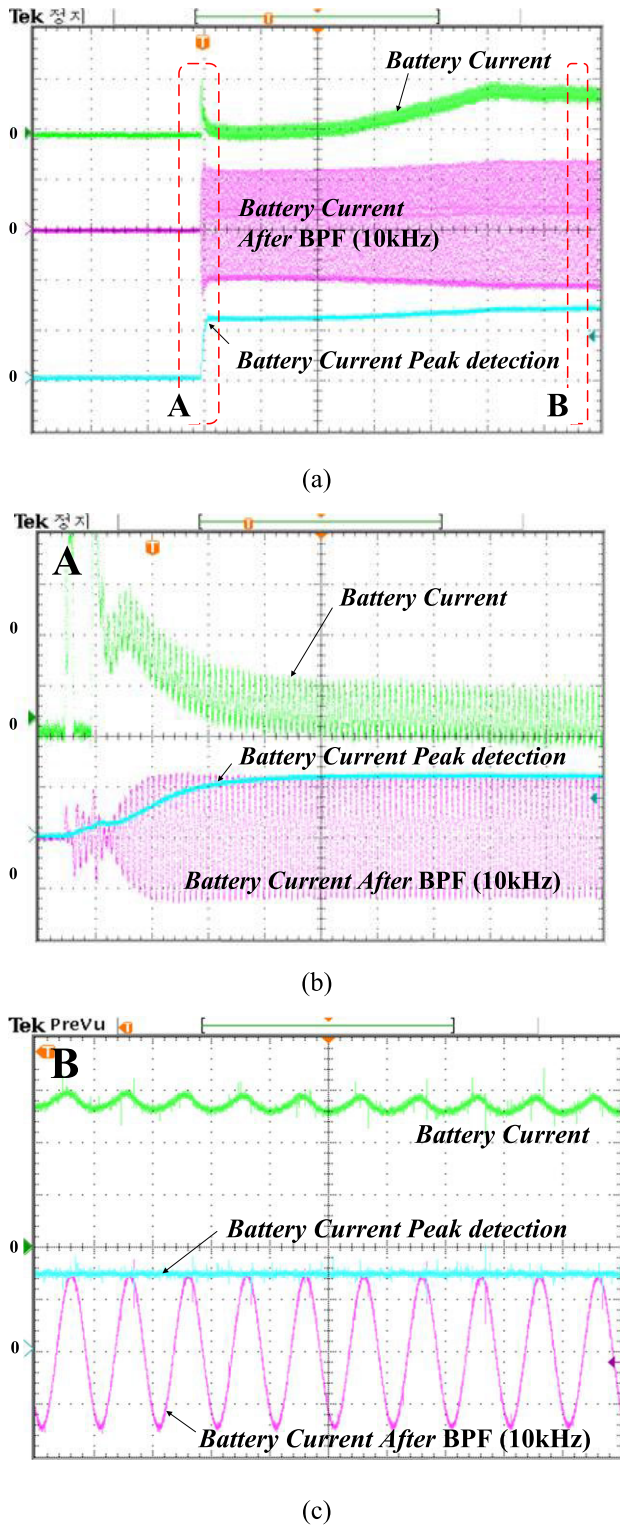
Charger (SMPS×4)		AC-IR Measurement Board	
Power Capacity	1.2 kW	Impedance Range	1~1,000mΩ
Charging Voltage	10~48 V	Measurable low frequency	1~1000 Hz
		High frequency	10~20 kHz
Charging Current-continuous	1~15 A	Operating Voltage-Max	48 V
CV charging method	Dual frequency	Measurement Current-Max	20 A
Charging Current Error	Below 5 %	Measurement Method	AC-IR



**FIGURE 18.** Separation of effective and reactive currents for estimating  $R_d$  and  $C_d$ .

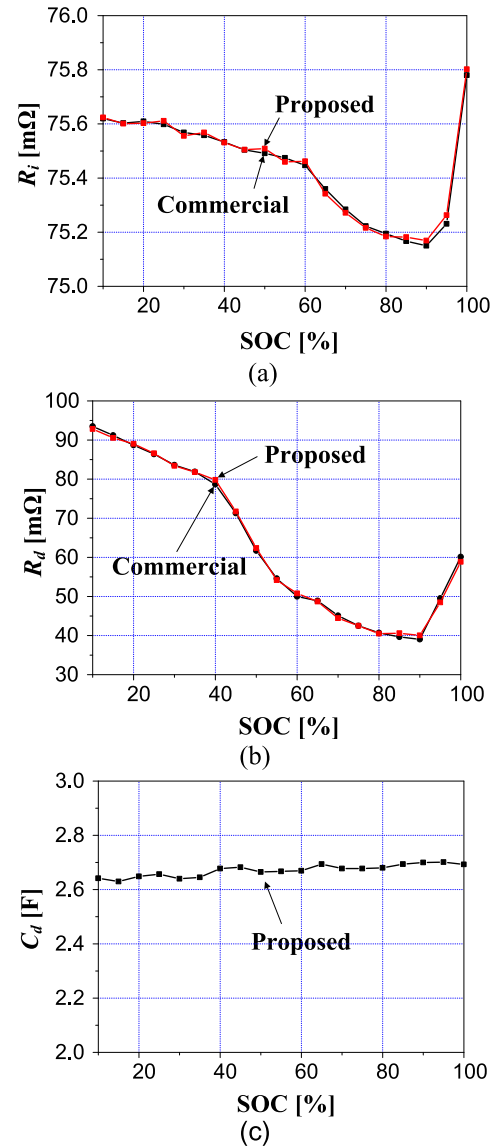
to effective current flowing in resistor in phase with and reactive current which has a phase difference of  $90^\circ$  with capacitor voltage, and then  $R_d$  (charge transfer resistance) and  $C_d$  (electric double layer capacitance) are estimated.

Fig. 19 shows the process of extracting high frequency of 10kHz using BPF, extracting fundamental wave, and extracting electrolyte resistance ( $R_i$ ) through peak value detection. If the injected frequency is infinite, the battery



**FIGURE 19.** Estimation of  $R_i$ , (a) Separation of high frequency and detection of maximum value, (b) Estimation of maximum value in transient state, (c) Estimation of maximum value in steady state.

impedance equals to  $R_i$ ; however, as infinite frequency is practically impossible, in this test,  $R_i$  is estimated by applying a high frequency power where capacitive reactance practically becomes zero. When the frequency is assumed to be



**FIGURE 20.** Parameter comparison with commercial instrument, (a)  $R_i$ , (b)  $R_d$ , (c)  $C_d$ .

a very high frequency where the capacitive reactance near to be zero, battery parameter  $R_i$  can be estimated by extracting peak value.

To verify the validity and accuracy of the proposed AC-IR parameter measurement method, battery parameters are measured according to IEC62133 using commercial products HIOKI BT3564 [26]–[28]. The average value through 50 repeated measurements is presented in Table 3. The experiment compares the measurements of  $R_i$  and  $R_d$  under 0.5C discharge conditions with the chamber temperature constant at 24°C and are given in Fig. 20(a) and 20(b), respectively. When comparing the error of the measurement results of the two methods,  $R_i$  is measured 0.24% and  $R_d$  is 1.18%, respectively. We can find that measurement error in electrolyte resistance ( $R_i$ ) is smaller than charge transfer resistance ( $R_d$ ). The  $C_d$  shown in Fig. 20(c) is not instrumented in BT3564 [28],

TABLE 3. Comparison of estimated values with BT3564.

SOC %	$R_i$		$R_d$		$C_d$
	BT3564	Proposed	BT3564	Proposed	Proposed
100	75.78	75.80	60.12	58.86	2.69
95	75.23	75.26	49.51	48.48	2.70
90	75.15	75.17	39.03	40.04	2.70
85	75.17	75.18	39.65	40.60	2.69
80	75.19	75.18	40.70	40.50	2.68
75	75.22	75.22	42.50	42.50	2.68
70	75.28	75.27	45.10	44.46	2.68
65	75.36	75.34	48.90	48.70	2.69
60	75.45	75.46	50.00	50.77	2.67
55	75.47	75.46	54.60	54.18	2.67
50	75.49	75.57	61.70	62.38	2.66
45	75.50	75.51	71.30	71.73	2.68
40	75.53	75.53	78.68	79.81	2.68
35	75.56	75.57	81.90	81.80	2.65
30	75.57	75.56	83.60	83.40	2.64
25	75.60	75.61	86.40	86.60	2.66
20	75.61	75.60	88.70	89.03	2.65
15	75.60	75.60	91.20	90.54	2.63
10	75.62	75.62	93.50	92.83	2.64

indicating only parameters by the method proposed in this paper.

## V. CONCLUSION

The proposed AC-IR parameter measurement estimates internal battery parameters using high and low frequencies, requiring a power converter that can supply AC ripple with DC offset wave. Using BPF, the electrolyte resistance ( $R_i$ ) is estimated by detecting AC components of a particular frequency voltage and current and entering very high frequencies that have the effect of short circuiting the equivalent capacitance by electric double layer ( $C_d$ ) of the Randles model. The charge transfer resistance ( $R_d$ ) and electrical double layer capacitance ( $C_d$ ) are estimated via DFT, which separates effective and reactive currents by entering a low frequency at which the phase difference between voltage and current is significant. To realize the proposed approach, we propose analog power measurements and peak detection circuits, and a circuit configuration of converter supplying AC ripple with DC offset wave to estimate internal parameters at the same time to charge battery.

To verify the validity and accuracy of the proposed AC-IR parameter measurement method, battery parameters are measured and compared according to IEC62133 using commercial products HIOKI BT3564 which is an expensive measurement equipment. As a result, we can find that the error rate compared to BT3564 is low as  $R_i$  is 0.24% and  $R_d$  is 1.18%, respectively.

## REFERENCES

- [1] Z. Xia and J. A. Abu Qahouq, "State-of-charge balancing of lithium-ion batteries with state-of-health awareness capability," *IEEE Trans. Ind. Appl.*, vol. 57, no. 1, pp. 673–684, Jan. 2021.
- [2] S. Cui and I. Joe, "A dynamic spatial-temporal attention-based GRU model with healthy features for state-of-health estimation of lithium-ion batteries," *IEEE Access*, vol. 9, pp. 27374–27388, Feb. 2021.
- [3] Z. Wang, C. Yuan, and X. Li, "Lithium battery state-of-health estimation via differential thermal voltammetry with Gaussian process regression," *IEEE Trans. Transp. Electrific.*, vol. 7, no. 1, pp. 16–25, Mar. 2021.
- [4] J. S. Goud, K. R., and B. Singh, "An online method of estimating state of health of a li-ion battery," *IEEE Trans. Energy Convers.*, vol. 36, no. 1, pp. 111–119, Mar. 2021.
- [5] L. Ling and Y. Wei, "State-of-charge and state-of-health estimation for lithium-ion batteries based on dual fractional-order extended Kalman filter and online parameter identification," *IEEE Access*, vol. 9, pp. 47588–47602, Mar. 2021.
- [6] Y. Gao, K. Liu, C. Zhu, X. Zhang, and D. Zhang, "Co-estimation of state-of-charge and state-of-health for lithium-ion batteries using an enhanced electrochemical model," *IEEE Trans. Ind. Electron.*, early access, Mar. 23, 2021, doi: 10.1109/TIE.2021.3066946.
- [7] J. Meng, L. Cai, D.-I. Stroe, X. Huang, J. Peng, T. Liu, and R. Teodorescu, "An automatic weak learner formulation for lithium-ion battery state of health estimation," *IEEE Trans. Ind. Electron.*, early access, Mar. 17, 2021, doi: 10.1109/TIE.2021.3065594.
- [8] T. Ouyang, P. Xu, J. Lu, X. Hu, B. Liu, and N. Chen, "Co-estimation of state-of-charge and state-of-health for power batteries based on multi-thread dynamic optimization method," *IEEE Trans. Ind. Electron.*, early access, Mar. 3, 2021, doi: 10.1109/TIE.2021.3062266.
- [9] N. Khan, F. U. M. Ullah, Afnan, A. Ullah, M. Y. Lee, and S. W. Baik, "Batteries state of health estimation via efficient neural networks with multiple channel charging profiles," *IEEE Access*, vol. 9, pp. 7797–7813, Dec. 2021.
- [10] Q. Huo, Z. Ma, X. Zhao, T. Zhang, and Y. Zhang, "Bayesian network based state-of-health estimation for battery on electric vehicle application and its validation through real-world data," *IEEE Access*, vol. 9, pp. 11328–11341, 2020.
- [11] W. Xiong, Y. Mo, and C. Yan, "Online state-of-health estimation for second-use lithium-ion batteries based on weighted least squares support vector machine," *IEEE Access*, vol. 9, pp. 1870–1881, Dec. 2021.
- [12] E. Schaltz, D.-I. Stroe, K. Norregaard, L. S. Ingvarsdn, and A. Christensen, "Incremental capacity analysis applied on electric vehicles for battery state-of-health estimation," *IEEE Trans. Ind. Appl.*, vol. 57, no. 2, pp. 1810–1817, Mar. 2021.
- [13] M. I. Wahyuddin, P. S. Priambodo, and H. Sudibyo, "Direct current load effects on series battery internal resistance," in *Proc. 15th Int. Conf. Qual. Res. (QiR): Int. Symp. Electr. Comput. Eng.*, Nusa Dua, Bali, Indonesia, Jul. 2017, pp. 24–27.
- [14] Z. He, D. Guo, X. Liu, and G. Yang, "An evaluation method of battery DC resistance consistency caused by temperature variation," in *Proc. 43rd Annu. Conf. IEEE Ind. Electron. Soc. (IECON)*, Beijing, China, Oct. 2017, pp. 7623–7628.
- [15] I. Kurisawa and M. Iwata, "Internal resistance and deterioration of VRLA battery-analysis of internal resistance obtained by direct current measurement and its application to VRLA battery monitoring technique," in *Proc. Power Energy Syst. Converging Markets*, Melbourne, VIC, Australia, 1997, pp. 687–694.
- [16] J. Hoon Kim, S. Jun Lee, J. Moon Lee, and B. Hyung Cho, "A new direct current internal resistance and state of charge relationship for the li-ion battery pulse power estimation," in *Proc. 7th International Conf. Power Electron.*, Daegu, South Korea, Oct. 2007, pp. 22–26.
- [17] L. Wildfeuer, N. Wassiliadis, C. Reiter, M. Baumann, and M. Lienkamp, "Experimental characterization of li-ion battery resistance at the cell, module and pack level," in *Proc. 14th Int. Conf. Ecol. Vehicles Renew. Energies (EVER)*, Monte-Carlo, Monaco, May 2019, pp. 8–10.
- [18] S.-J. Kwon, J. Kim, J. H. Choi, J.-H. Lim, and S. Lee, "Comparative analysis of NCM LIB equivalent parameter according to AC-DC impedance estimation method," in *Proc. 10th Int. Conf. Power Electron. ECCE Asia (ICPE-ECCE Asia)*, Busan, South Korea, May 2019, pp. 27–30.
- [19] W. Liu, X. Sun, H. Wu, Z. He, and G. Yang, "A multistage current charging method for li-ion battery bank considering balance of internal consumption and charging speed," in *Proc. IEEE 8th Int. Power Electron. Motion Control Conf. (IPEMC-ECCE Asia)*, Hefei, China, May 2016, pp. 22–26.
- [20] A. Lievre, A. Sari, P. Venet, A. Hijazi, M. Ouattara-Brigaudet, and S. Pelissier, "Practical online estimation of lithium-ion battery apparent series resistance for mild hybrid vehicles," *IEEE Trans. Veh. Technol.*, vol. 65, no. 6, pp. 4505–4511, Jun. 2016.
- [21] B. Balagopal, C. S. Huang, and M.-Y. Chow, "Sensitivity analysis of lithium ion battery parameters to degradation of anode lithium ion concentration," in *Proc. 45th Annu. Conf. IEEE Ind. Electron. Soc. (IECON)*, Lisbon, Portugal, Oct. 2019, pp. 14–17.

- [22] S. Viridi, Hendro, and F. Pasila, "Fast charging batteries simulation based on capacitor model change of resistance due to internal deposition," in *Proc. Electr. Power, Electron., Commun., Controls Informat. Seminar (EECCIS)*, Batu, Indonesia, Oct. 2018, pp. 9–11.
- [23] R. Zhao, L. Zhai, J. Liu, and J. Gu, "Experimental studies on battery low-temperature behaviors and two heating approaches," in *Proc. Int. Conf. Sensing, Diagnostics, Prognostics, Control (SDPC)*, Xi'an, China, Aug. 2018, pp. 15–17.
- [24] Q. Guo, W. Qu, H. Deng, X. Zhang, Y. Li, X. Wang, and X. Yan, "Estimation of electric vehicle battery state of health based on relative state of health evaluation," in *Proc. IEEE 2nd Adv. Inf. Technol., Electron. Autom. Control Conf. (IAEAC)*, Chongqing, China, Mar. 2017, pp. 25–26.
- [25] M. Zuniga, J. Jaguemont, L. Boulon, and Y. Dube, "Heating lithium-ion batteries with bidirectional current pulses," in *Proc. IEEE Vehicle Power Propuls. Conf. (VPPC)*, Montreal, QC, Canada, Oct. 2015, pp. 19–22.
- [26] *Secondary Cells and Batteries Containing Alkaline or Other Non-Acid Electrolyte—Safety Requirements for Portable Sealed Secondary Cells, and for Batteries Made From Them, for Use in Portable Application—Part 2: Lithium Systems*, document IEC62133, 2020.
- [27] *Electrical Measurements of Lithium-Ion Batteries—Fundamentals and Applications, User's Guide*, HIOKI, Nagano, Japan, 2020.
- [28] *High Voltage Battery Tester for EV and PHEV, BT3564 Data Sheet*, HIOKI, Nagano, Japan, 2019.



**KWANG SEOK SONG** received the B.S., M.S., and Ph.D. degrees in electrical engineering from Chonnam National University, Gwangju, South Korea, in 1997, 2008, and 2021, respectively. Since 2013, he has been a CTO with LTOP Company Ltd., Gwangju. His research interest includes power conversion systems such as, battery management systems, and battery charger.



**SUNG-JUN PARK** received the B.S., M.S., and Ph.D. degrees in electrical engineering, and the Ph.D. degree in mechanical engineering from Pusan National University, Busan, South Korea, in 1991, 1993, 1996, and 2002, respectively. From 1996 to 2000, he was an Assistant Professor with the Department of Electrical Engineering, Koje College, Koje, South Korea. From 2000 to 2003, he was an Assistant Professor with the Department of Electrical Engineering, Tongmyong College, Busan. Since 2003, he has been a Professor with the Department of Electrical Engineering, Chonnam National University, Gwangju, South Korea. His research interests include power electronics, motor control, mechatronics, and micromachine automation.



**FEEL-SOON KANG** (Member, IEEE) received the M.S. and Ph.D. degrees in electrical engineering from Pusan National University, South Korea, in 2000 and 2003, respectively. Since 2003, he had been with the Department of Electrical Engineering, Osaka University, Japan, as a Post-doctoral Fellow. Since 2004, he has been with the Department of Electronic Engineering, Hanbat National University, South Korea, as a Professor. His research interests include power electronics including, design, control, and reliability analysis of various power conversion systems for photovoltaic power generation systems, electric vehicles, and HVDC systems. He is a member of KIEE and KIPE. He received the Student Award and the Best Presentation Prizes from the IEEE Industrial Electronics Society, in 2001, and he was honored with the Academic Awards from Pusan National University, in 2003 and Hanbat National University, in 2005. He also received the several best paper awards from The Korean Institute of Electrical Engineers (KIEE) and The Korean Institute of Power Electronics (KIPE). He served as the Vice-Chairman of the Organizing Committee for the International Telecommunications Energy Conference (IEEE Intelec 2009), IEEE Vehicle Power and Propulsion Conference (IEEE VPPC 2012), IEEE Transportation Electrification Conference and Expo (IEEE ITEC 2016), International Conference on Electrical Machines and Systems (ICEMS 2010, 2013, and 2018) and as a Secretary of International Conference on Magnetically Levitated Systems and Linear Drives (Maglev 2011). He served as an Associate Editor for the IEEE TRANSACTIONS ON INDUSTRIAL ELECTRONICS, from 2004 to 2011.

...